Kinetic mechanisms of the C49-to-C54 polymorphic transformation in titanium disilicide thin films: A microstructure-scaled nucleation-mode transition

Z. Ma and L. H. Allen
Department of Materials Science and Engineering and Coordinated Science Laboratory, University of Illinois at Urbana-Champaign, Urbana, Illinois 61801

(Received 16 November 1993)

The kinetics and mechanism of the polymorphic transformation in titanium disilicide thin films from a base-centered orthorhombic structure ($C49$-$TiSi_2$) to a face-centered orthorhombic structure ($C54$-$TiSi_2$) were investigated with the emphasis on the effect of film thickness scaling on the phase transition using *in situ* resistance measurements, x-ray diffraction, and transmission electron microscopy (TEM). The $C49$ disilicide films of different thicknesses were prepared by annealing Ti/polycrystalline Si thin film couples of varying Ti thicknesses (250, 550, and 1000 Å). The transformation rate was found to be a strong function of the film thickness and temperature, and can be described by $\tau \propto \exp(E_a/kT)$ with an activation energy of $E_a = 3.73$, 4.44, and 5.08 (± 0.07) eV for 1000, 550, and 250 Å Ti, respectively. An unusual transition between nucleation sites was observed as a result of the scaling: for samples with 250 Å Ti, the transformation proceeded by nucleating the $C54$ polymorph at grain edges (three-grain junctions) of the $C49$-$TiSi_2$ films while the $C54$ nuclei were predominantly formed at the grain boundaries (two-grain junctions) in thicker films, which are in good agreement with the predictions of the nucleation mode from kinetics analyses. It has been suggested that the nucleation of the $C54$-$TiSi_2$ is likely to be the rate-limiting step in the overall transformation. Based upon the microstructural evidences provided by TEM analyses, the significance of these observations due to the reduction in film thickness was discussed by considering energetics of nucleation at different geometrical sites, nucleation site density, and effects of surface and stress. It was demonstrated that the surface contribution and nucleation site density become important for nucleation in thinner films with largely increased surface-to-volume ratio. The nucleation-mode transition is driven by the morphological and microstructural changes associated with thickness scaling.

I. INTRODUCTION

In recent years, the development of ultra-large-scale integrated circuits technology has been characterized by an impressive move towards higher packing density and enhanced device performance. As feature sizes of integrated circuits scale down, the associated geometries impose severe restrictions on the junction depth. This, in turn, requires a compatible scaling of the interconnection lines based upon the classical laws of scaling as introduced by Dennard *et al.*[1] It has been shown that such dimensionality change brings about a lot of challenge and complexity in the manufacturing of integrated circuits.[2-4] Some issues such as stress-induced voiding[5] and stress-induced structural instability,[6] which are obscured in thicker films, emerge as important limiting factors receiving serious attention. In order to successfully fabricate and control ultrashallow junctions under these restrictions, the existing microelectronic processes need to be reassessed and the underlying mechanisms involved in these processes must be well understood.

Refractory titanium disilicide with a face-centered orthorhombic structure (designated $C54$-$TiSi_2$) is currently being used in the self-aligned silicidation (known as SALICIDE) technology because of its low resistivity ($13 \sim 20$ $\mu\Omega$ cm), good thermal stability and structural compatibility. In this process, the silicide is simultaneously formed on the source, drain, and gate regions of metal-oxide semiconductor field-effect transistors (MOSFET), thereby avoiding high parasitic series resistance and high contact resistance between the metallization and the devices. It is usually prepared through a Ti/Si bilayer reaction[7,8] or crystallization of codeposited stoichiometric amorphous alloys.[9,10] However, due to kinetic constraints, in both cases, a high resistivity ($80 \sim 100$ $\mu\Omega$ cm) metastable disilicide always appears first as an intermediate phase before the stable $C54$ phase forms.[9,11,12] This metastable phase is composition invariant to the $C54$ phase and possesses a base-centered orthorhombic structure. It is crystallographically isomorphous to $ZrSi_2$ ($C49$ structure) and is often heavily faulted along the $[0k0]$ direction.[13] The $C49$-to-$C54$ polymorphic transformation occurs upon a high-temperature anneal (above 650 °C) and is monotropical under ordinary pressure.

Because the $C49$-to-$C54$ structural transition is an inevitable way to achieving the required disilicide, this transformation has been the subject of extensive studies from technological as well as scientific viewpoints. There have been some research activities on optimizing the silicide properties by promoting epitaxy[14,15] and changing processing schemes.[16] It has been reported that the transformation to the low resistivity $C54$ phase is affected by the type of dopant involved and is hindered on heavily doped n-type silicon substrates.[8,17] Recently, Lasky *et al.*[2] have shown very interesting results about the

0163-1829/94/49(19)/13501(11)/$06.00 ©1994 The American Physical Society

influence of line width on the $C49$-to-$C54$ transformation and found that the structural transition is significantly retarded on submicron lines. They suggested that more nucleation events for the $C54$ phase were required to completely transform narrow lines. Since these issues are of increasing technological importance for developing silicided, ultra shallow junctions in MOS transistors, it is extremely desirable to provide additional fundamental understanding of the nucleation behavior of the stable $C54$ disilicide and the $C49$-to-$C54$ phase transformation kinetics. Although there are some reports concerning the kinetics of this transformation, they are focused on the effects of dopant and substrates.[10] Furthermore, the influence of scaling on the phase transition is of fundamental interest. As film thickness decreases, surface and stress contributions to phase transition become more prominent due to large increase in surface-to-volume ratio. It is the purpose of this paper to address the general question of how these subtle changes, such as film thickness, will affect the rate of this polymorphic transformation and its detailed kinetic behavior.

In this paper, we describe a detailed kinetics study on the $C49$-$TiSi_2$-to-$C54$-$TiSi_2$ structural transformation from a Ti/polycrystalline Si bilayer reaction and the influence of the film thickness on the kinetic rates. Kinetic analyses are also closely correlated with the initial microstructural evolution of the polymorphic change, as revealed by transmission electron microscopy (TEM) and transmission electron diffraction. It is demonstrated that the transformation temperature increases with decreasing film thickness as manifested by an increase in activation energy for the transformation. As the film thickness is reduced, a transition between available nucleation sites for the $C54$ phase is observed. The physical origin of these changes are discussed in terms of the energetic consideration for nucleation at different sites, nucleation site density, and effects of surface and stress.

II. EXPERIMENTAL PROCEDURES

To facilitate the kinetics study, the samples used in this work were prepared in a special geometry to allow *in situ* measurement of the film sheet resistance while annealing (the background of this method will be discussed in the next section). A 750-nm-thick oxide was first thermally grown on *p*-type Si (100) wafers. Then, a layer of phosphorus doped polycrystalline Si (poly-Si) film was grown onto the oxidized Si wafers using low-pressure chemical vapor deposition. The wafers were then chemically cleaned by dipping in a dilute HF solution just prior to loading into a rf sputtering deposition chamber with a base pressure of about 2×10^{-8} Torr. Titanium films of different thicknesses (250, 550, and 1000 Å, designated as samples A, B, and C, respectively, thereafter) were deposited over the pregrown polycrystalline Si. The samples so constructed are suited for the following *in situ* sheet resistance measurement. The thermal oxide here serves as the electrical isolation between the films and the Si substrate. The Ti films were checked for possible contaminations using Auger electron spectroscopy. Both C and O were not detectable after removal of a surface contaminated layer.

Studies of the transformation kinetics were carried out under isothermal annealing condition in a temperature range from 640 to 740 °C. Because the Ti/Si reaction goes through the formation of an amorphous silicide (a-$TiSi_x$) before forming the $C49$ phase,[11,18] the samples were first annealed to allow all the Ti films to be consumed and converted into the metastable $C49$ phase. An *in situ* resistance measurement was carried out to follow the reaction path in order to avoid any $C49$-to-$C54$ transformation in this process. This was also double checked by TEM and x-ray diffraction. Isothermal annealing was performed in a programmable tube furnace with a base pressure of 5×10^{-8} Torr. During annealing, the $C49$-to-$C54$ transition occurred and the film sheet resistance was measured *in situ* with four spring-loaded molybdenum probes arranged in a Van der Pauw geometry. As demonstrated in our previous papers,[11,19] such an *in situ* measurement is capable of providing timely information about the progress of a thin-film reaction by monitoring the change of the film resistance and the change of the temperature coefficient of resistance. Due to the distinct resistance decrease associated with the $C49$-to-$C54$ polymorphic transformation, the progress of the phase change can be easily tracked. Also, with the aid of the *in situ* resistance probe, we are able to obtain the critical samples which have been annealed to various stages for *ex situ* analysis simply by interrupting annealing at specific times and then allowing them to rapidly cool down to ambient temperature. A few samples were obtained this way for studying the initial stage of the microstructure change.

Microstructural studies of the phase transformation were carried out using x-ray diffraction (XRD) and transmission electron microscopy (TEM) observed both in cross section and plan view. Plan-view TEM specimens were prepared by backside mechanical polishing down to ~30 μm, followed by ion milling with a liquid-nitrogen cold trap to electron perforation. Cross-sectional TEM specimens were made by following standard procedures of face-to-face gluing, mechanical thinning, and cold trap ion milling with an ion-beam incident angle of $12°\sim15°$. XRD measurements were carried out on a Rigaku D/Max III A diffractometer using Cu $K\alpha$ radiation. TEM examinations were performed in a Philips CM-12 transmission electron microscope operated at 120 kV as well as a Hitachi H-9000 transmission electron microscope operated at 300 kV. Microstructure of the $C49$ and $C54$ phases was identified using selected area electron diffraction and electron microdiffraction.

III. RESULTS

A. Microstructure of $C49$-$TiSi_2$ prior to transforming to $C54$-$TiSi_2$

Before studying the polymorphic transformation, the microstructure and morphology of the metastable $C49$-$TiSi_2$ were examined using plan-view and cross-sectional TEM. Figures 1(a), 1(b), and 1(c) (left) show planar view micrographs of the polycrystalline $C49$ phase formed

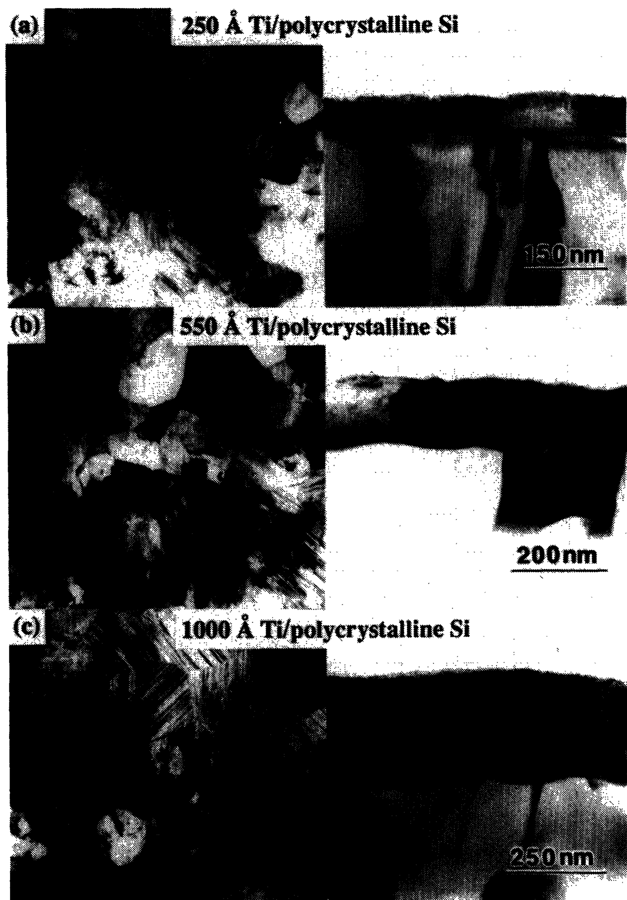

FIG. 1. Plan-view (left) and cross-sectional (right) TEM micrographs of the $C49$-$TiSi_2$ films formed by reacting poly-Si with Ti films of different thicknesses, showing the microstructure and morphology of the $C49$-$TiSi_2$ prior to transforming to the $C54$-$TiSi_2$. (a) 250 Å Ti, (b) 550 Å Ti, and (c) 1000 Å Ti.

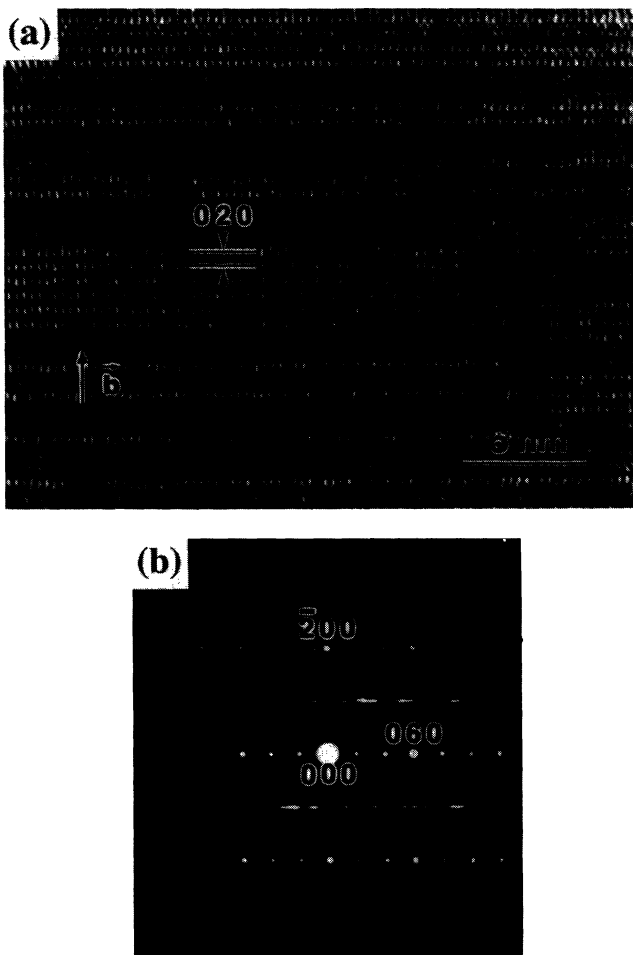

FIG. 2. (a) High-resolution TEM micrograph of the defective $C49$-$TiSi_2$ structure viewed along [100] axis. The stacking faults in **b** direction are revealed. The planes are often displaced by a vector $1/2(\mathbf{a}+\mathbf{c})$. (b) a typical [100] selected area electron-diffraction pattern.

from bilayers of 250 Å Ti/poly-Si, 550 Å Ti/poly-Si, and 1000 Å Ti/poly-Si, respectively. Figures 1(a), 1(b), and 1(c) (right) are a set of cross-sectional TEM micrographs of the corresponding samples. Except for some surface oxide (presumably titanium oxide), all the Ti films have reacted with polycrystalline Si, resulting in a continuous layer of polycrystalline $C49$ titanium disilicide, as identified using electron diffraction and XRD. The average grain size of the $C49$ phase is about 1500 Å for sample A, about 1800 Å for sample B, and 2300 Å for sample C. As seen in both plan-view and cross-sectional images, the metastable $C49$ disilicides are heavily faulted. A close examination reveals that the planes along the **b** direction of the base-centered orthorhombic unit cell are usually improperly stacked, being displaced by $1/2(\mathbf{a}+\mathbf{c})$.[13] The highly-faulted structure of the $C49$-$TiSi_2$ can be perceived along the [100] or [001] projections [Fig. 2(a)]. Its corresponding electron-diffraction pattern is shown in Fig. 2(b). The defective nature of the $C49$ phase is believed to be partially responsible for the high resistive behavior.

It is noticed from the cross-sectional views of the $C49$ microstructure that the $C49$ phases formed via 250 Å Ti/poly-Si and 550 Å Ti/poly-Si bilayer reactions (samples A and B) are essentially a layer of two-dimensional polycrystalline structure sitting on the remaining poly-Si with the grain boundaries running through the entire film thickness. Grain-boundary grooving is also observed in two cases with sample A more severe than sample B. On the contrary, the $C49$ microstructure consists of more than one layer of polycrystalline grains formed over poly-Si in sample C. It will be shown that these different microstructure features will dramatically affect the following polymorphic transformation.

B. *In situ* resistance measurement

As mentioned previously, the metastable $C49$-$TiSi_2$ and stable $C54$-$TiSi_2$ have quite different values of film resistivity. When the $C49$-$TiSi_2$ film is isothermally annealed in a suitable temperature range, it gradually transforms to the stable $C54$ disilicide and the film resistance continuously drops down with annealing time, i.e., $R=f(t)$, due to the increase in volume fraction of the low resistivi-

ty $C54$ phase formed by consuming high resistivity $C49$ phase. This distinct characteristic provides us a convenient probe for quantitatively measuring the kinetic process of this polymorphic transformation. Figure 3 presents normalized resistance plots as a function of isothermal annealing time for different samples. For the sake of clarity, only three temperatures are shown in each figure, although at least six different temperatures were used for each type of sample. To observe the phase transformation within a reasonable time frame, a feasible temperature window was selected for each type of sample.

In order to relate the change in resistance to the progress of the polymorphic transition, a resistance model is adopted to define the volume fraction of the $C49$ phase which has transformed into the $C54$ phase,

$$X_T(t)=\frac{R(0)-R(t)}{R(0)-R(f)} \tag{1}$$

in terms of the initial film resistance of the $C49$ phase $R(0)$, final film resistance of the $C54$ phase $R(f)$, and time-dependent film resistance $R(t)$. This model has been successfully used to describe various kinds of kinetic events such as precipitation process,[20,21] crystallization,[10,22] and recrystallization processes,[23] *etc.* The curves plotted in Fig. 4 are obtained from the resistance data shown in Fig. 3 using Eq. (1). These plots exhibit

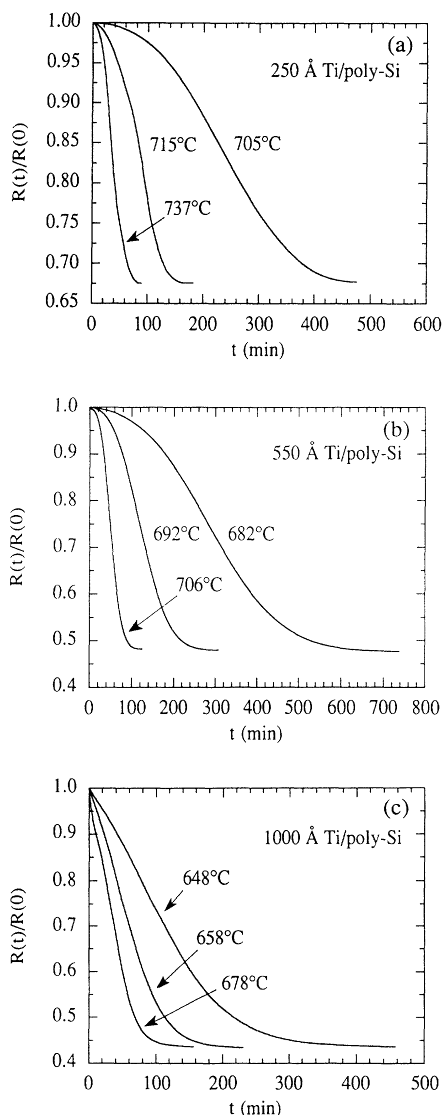

FIG. 3. Normalized resistance plots as a function of isothermal annealing time at different temperatures for three types of samples. (a) 250 Å Ti/poly-Si, (b) 550 Å Ti/poly-Si, and (c) 1000 Å Ti/poly-Si.

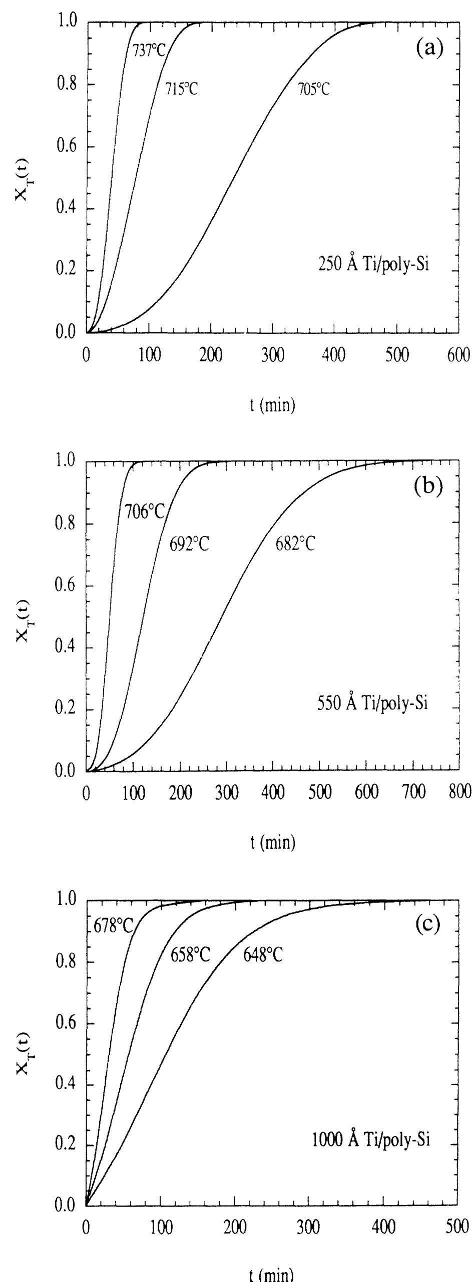

FIG. 4. Transformation curves at different isothermal temperatures derived from the data shown in Fig. 3 using Eq. (1). (a) 250 Å Ti/poly-Si, (b) 550 Å Ti/poly-Si, and (c) 1000 Å Ti/poly-Si.

sigmoidal shapes, suggesting that the transformation is accomplished by a nucleation and growth mechanism. It is observed that for the same film thickness (Ti film thickness or effective thickness of the $C49$ disilicide film), the time required to complete the transformation decreases with increasing isothermal annealing temperature. Also, as the film thickness is reduced, the transformation temperature increases. The temperature difference in initiating the $C49$-to-$C54$ structural transition can be as large as $\sim 50\,^{\circ}\mathrm{C}$ due to the change in film thickness in our samples.

The rate of the polymorphic transformation is often gauged by the so-called transformation velocity,[24] which is defined as the first derivative of the volume fraction transformed $X_T(t)$ with respect to time t, i.e., $dX_T(t)/dt$. In this case $dX_T(t)/dt$ represents the rate at which the parent phase ($C49$-$TiSi_2$) has transformed to the product phase ($C54$-$TiSi_2$). A typical plot of transformation velocity versus time under isothermal anneal condition is given in Fig. 5. The transformation velocity is also a variable and depends upon temperature and time. In a first half-time period, the rate of the $C49$-to-$C54$ transition increases with time. After reaching a maximum velocity, the transformation slows down monotonically. To measure the kinetic difference caused by the change of sample thickness, the transformation rates at 20% of the $C49$ disilicide having been converted to the $C54$ disilicide, i.e., $X_T(t)=0.2$, were calculated for three types of samples and are plotted in Fig. 6 against the reciprocal of temperature. Two important results can be drawn from this figure: (1) the transformation rates increase with increasing annealing temperature, indicating that the transformation is thermally activated; (2) higher annealing temperatures are required for thinner films to reach the same rates as those for thicker films.

From a kinetics viewpoint, the rate of a polymorphic transformation depends upon the energy barrier opposing the process. In other words, a certain thermal activation is necessary to cause the transformation to proceed. Therefore, it would be useful to deduce these quantities for three different types of samples in order to understand the rate difference. To do this, a Johnson-Mehl-Avrami-type of kinetic analysis[25] was used. According to their

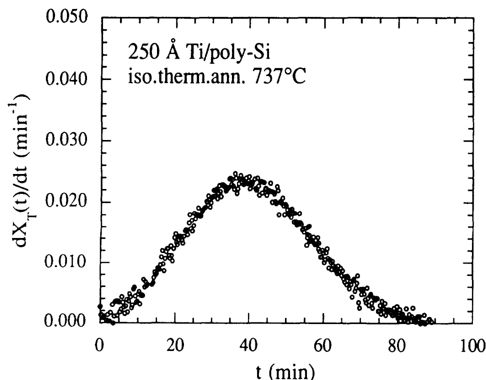

FIG. 5. A typical plot of transformation velocity vs annealing time under isothermal condition.

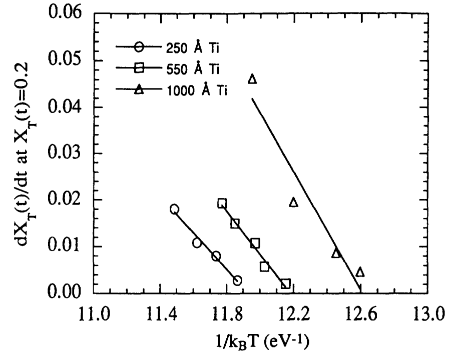

FIG. 6. Transformation velocity at $X_T(t)=0.2$ vs the reciprocal of annealing temperature for three different types of samples.

formulation, the volume fraction transformed can be described by

$$X_T(t)=1-\exp(-X_{\mathrm{ext}}) , \tag{2}$$

where X_{ext} is the extended volume fraction of the $C54$ disilicide and can be expressed as

$$X_{\mathrm{ext}}=bt^n , \tag{3}$$

where b is a kinetic parameter, depending on the nucleation rate and growth rate of the disilicide, n is a mode parameter of the polymorphic transformation, generally implying the mode of nucleation or the dimensionality of growth, and t is the reaction time. If the half-time criterion is used,[10,22] i.e., by defining

$$X_T(\tau)=\tfrac{1}{2} \tag{4}$$

and

$$\tau=\tau_0\exp(E_a/k_BT) , \tag{5}$$

where k_B is the Boltzmann constant and T is temperature in K, an effective activation energy E_a for the transformation can be derived. In general, this activation energy is a combination of the activation energies for nucleation and growth, and is determined by the particular kinetic processes involved.[26,27] By plotting $\ln(\tau)$ versus $1/k_BT$, the slopes of these Arrhenius plots (Fig. 7) give the effective

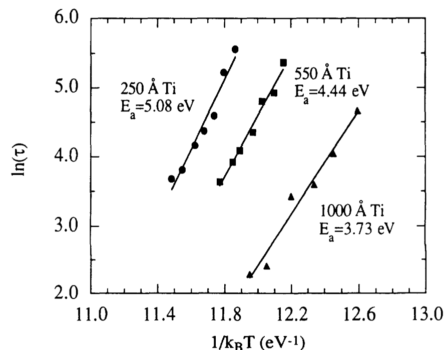

FIG. 7. Arrhenius plots of $\ln(\tau)$ vs $1/k_BT$ to determine activation energies for the transformation for three different types of samples. The parameter τ is the time required to complete 50% of the transformation.

activation energies of 5.08, 4.44, and 3.73 eV (± 0.07 eV) for the polymorphic transformation of samples A, B, and C, respectively. It is clearly seen that the activation energy increases with decreasing the film thickness.

Since these activation energies merely reflect the overall kinetic barriers opposing the transformation, it is desirable to know the detailed nucleation and growth behaviors which may cause the difference observed. By manipulating Eqs. (2), (3), and (4), one obtains

$$\ln\left\{-\frac{\ln[1-X_T(t)]}{\ln 2}\right\}=n\ln\left[\frac{t}{\tau}\right]. \quad (6)$$

Figure 8 is obtained by plotting the double natural logarithm term on the left-hand side versus $\ln(t/\tau)$. The n values specifying the nucleation mode can be extracted from the slopes of these plots. The averages of all the n values for samples A, B, and C are 2.13 ± 0.15, 1.82 ± 0.18, and 1.16 ± 0.12, respectively. The meaning of different n values for the polymorphic transformation is provided by Christian,[25] and has been explicitly derived and discussed by Cahn[28] and Vandermeer and Masumura.[29] A value of n close to 2 for samples A and B predicts a heterogeneous nucleation of the $C54$ phase predominantly at the grain edges (three-grain junctions) of the $C49$ phase, while $n\approx 1$ for sample C implies that the $C54$ nuclei predominantly formed at the $C49$ grain boundaries (two-grain junctions or normal grain boundaries).[28]

C. Nucleation of $C54$-$TiSi_2$

Although the kinetics analyses indicate that different nucleation modes of the stable $C54$ disilicide are involved in three types of samples used in this study, further microstructural characterizations are critically needed to substantiate these predictions. To investigate the nucleation behavior of the $C54$ disilicide, we obtained a set of samples (A, B, and C) which had been annealed to different stages of the transition in a way described in Sec. II and examined them using plan-view and cross-

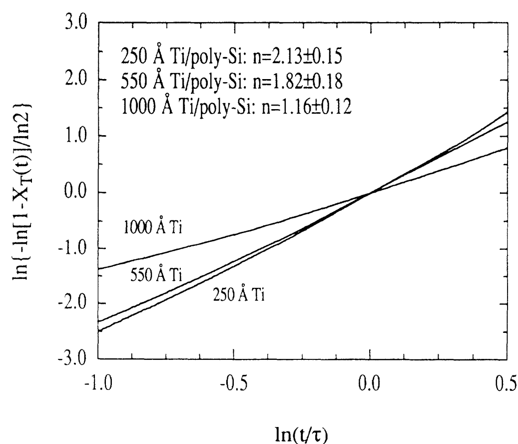

FIG. 8. Log-log plots to determine the mode of nucleation for the polymorphic transformation. The mode n is 2.13 ± 0.15, 1.82 ± 0.18, and 1.16 ± 0.12 for samples with 250, 550, and 1000 Å Ti, respectively.

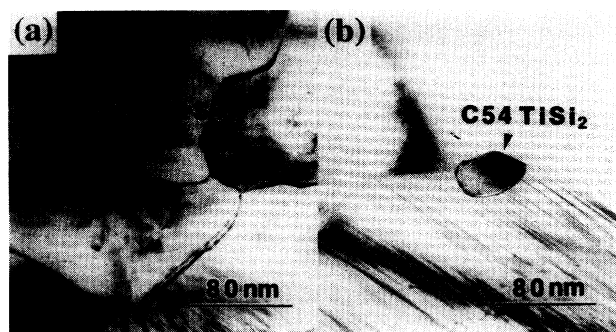

FIG. 9. Typical micrographs showing the location of the $C54$-$TiSi_2$ nuclei inside the $C49$-$TiSi_2$ thin films formed from samples with (a) 250 Å Ti (sample A) and (b) 1000 Å Ti (sample C). The $C54$ nuclei were identified using electron microdiffraction as well as dark-field imaging, and are indicated by arrows.

sectional TEM. Figures 9(a) and 9(b) are typical plan-view TEM micrographs taken from samples A and C, respectively. Selected area electron diffraction, electron microdiffraction, and dark-field imaging were used to identify and locate the $C54$ nuclei. The $C54$ disilicides were observed indeed to nucleate at the $C49$ grain edges in sample A and to predominantly form at their grain boundaries in sample C, which are quite consistent with the kinetics analysis. It is noted that in sample C the $C54$ nuclei were also found at the $C49$ grain edges but the density of the nuclei occurring at grain boundaries is higher than that at grain edges.

It is interesting to note from cross-sectional TEM observations that most of the $C54$ nuclei were found inside the parent $C49$ phase. At least at the early stages of the transformation, the $C54$ phase was not found at the interface between $C49$-$TiSi_2$ and poly-Si, being quite selective. We have also noticed that the density of the nuclei is rather low in these samples. In some areas of the TEM specimens, extremely large $C54$ grains were found while the others remained untransformed. It was difficult to find an area where the $C49$ phase has only partially transformed to the $C54$ phase.

IV. DISCUSSION

The effect of Ti film thickness on the $C49$-to-$C54$ polymorphic transition was initially reported by Houtum and Raaijmakers[30] and later by Joen *et al.*[31] They observed that the threshold temperature for the $C49$-to-$C54$ transformation increases with decreasing film thickness. But the kinetics aspect and mechanism of this transition as related to the film thickness was not addressed. In this study, we have formally treated the effect of the initial Ti or $C49$ disilicide film thickness on the kinetics of the polymorphic transformation and observed the increasing difficulty of the structural transition due to the reduction of the film thickness. The significance of these influences is more pronouncedly represented by the deduced kinetic parameters: transformation velocity and effective activation energy. It is found that with reducing the film thick-

ness the activation energy increases. Also accompanying this scaling, the nucleation sites for the *C*54 phase switch from grain boundaries (a site of high dimensionality) to grain edges (a site of low dimensionality) of the parent *C*49 phase.[28]

Several groups have investigated the kinetics of the *C*49-to-*C*54 polymorphic transformation. Thompson *et al.*[10] obtained an activation energy of 4.45 eV for this transition. Li *et al.*[32] studied the effect of Sb on the phase transformation and reported reduced activation energies of 4.4, 3.5, and 2.9 eV for the films with 0.3, 1.3, and 2.5 at. % Sb, respectively. In this work, we have obtained increased activation energies of 3.73, 4.44, and 5.08 eV for samples with 1000, 550, and 250 Å Ti, respectively. Comparing these data, there is a very good agreement between activation energy of sample *B* (with 550 Å Ti) and those in Refs. 10 and 32. With increasing or reducing the Ti thickness, we observed a reduction or an increase of the activation energy by several tenths of 1 eV. It has been mentioned previously that the activation energy deduced represents the overall kinetic barrier to the transformation. To unravel the cause of these changes, it is useful to separate the overall process of the *C*49-to-*C*54 transition into the nucleation and growth of the *C*54 disilicide and consider them individually. Since polymorphic transformation is commonly described as a diffusional transformation involving short-range atom transfer across the moving interface separating the parent phase from the product phase and proceeds by the nucleation and growth of the product phase,[24,25] this type of decomposition is physically feasible.

Let us first get an idea about the rate-limiting step of this phase transition. Comparing two crystal structures of titanium disilicide,[9,33,34] the *C*54 phase is more closely packed than the *C*49 phase with about 6% volume difference. In both structures, the Ti atoms are sitting inside the hexagonal network of Si atoms in the basal planes with a tenfold coordination of Si atoms; but the Ti-Si bond lengths are somewhat larger in the *C*49 phase. These features imply that the difference in chemical free energy is very small. The driving force for the *C*49-to-*C*54 transition should be mainly due to the large entropy term associated with the *C*54 phase. Because no reliable heats of formation data[34,35] are available for the *C*49 and *C*54 disilicides, we cannot obtain accurate information about the driving force of the transformation. However, according to numerous reports on the polymorphic transformation of intermetallic compounds, the heat effects are determined to be rather small, ranging from 0.01 to 0.03 eV/atom.[36] In view of this, we believe that the driving force is also very small for the *C*49-to-*C*54 polymorphic transformation. Because nucleation of a polymorphic phase often takes place by the reconstruction of the parent phase and creates new interfaces (or surfaces), the generated new surface (or interfacial) energy along with the misfit strain energy caused by interfacial coherency are the main energy barriers to be overcome in order to successfully nucleate a new phase in the solid-state materials. Under such small driving forces, we suggest that the nucleation of the *C*54 phase is troublesome and is very likely the rate-limiting step in the whole transformation. Our observations of a few *C*54-$TiSi_2$ nuclei and large growth rate seem to support this argument. Nucleation-limited transformation phenomena have been reported in many systems.[37,38] In these cases, the nucleation event is very sensitive to the geometry of the nucleation sites, the density of nucleation sites, and surface and stress effects due to the small difference in bulk free energy between the parent phase and product phase but the growth occurs very fast. We suggest that most of the extra energy barrier revealed from the kinetics analysis comes from the increasing difficulty for the nucleation of the *C*54-$TiSi_2$ as the film thickness is scaled down. In the following, we consider several factors which may affect the nucleation and growth of the *C*54 phase and cause the observed increase in activation energy and change in nucleation sites.

A. Energetics of heterogeneous nucleation at different geometrical sites

It is expected that because of the small bulk free-energy difference between *C*49-$TiSi_2$ and *C*54-$TiSi_2$ the nucleation of the *C*54 phase is mostly heterogeneous in order to reduce the energy barrier opposing the nucleation event. At these sites the grain boundary that is eliminated by formation of a nucleus provides some of the needed critical energy for nucleation, thereby reducing the amount to be supplied by thermal activation. Clemm and Fisher[39] noticed that even with heterogeneous nucleation there are different barriers associated with different geometrical sites. According to their derivation and assuming isotropic grain-boundary energy, the energy barrier to be surmounted for nucleating the *C*54-$TiSi_2$ at different sites can be summarized as

$$\Delta G^* = \frac{4}{27}\frac{(b\sigma_{C49/C54} - a\sigma_{C49/C49})^3}{c^2(\Delta G_V - \Delta G_S)^2} , \tag{7}$$

where $\sigma_{C49/C54}$ is the interfacial energy between *C*49-$TiSi_2$ and *C*54-$TiSi_2$, $\sigma_{C49/C49}$ is the grain-boundary energy of the *C*49-$TiSi_2$, ΔG_V is the difference in volume free energy between *C*49-$TiSi_2$ and *C*54-$TiSi_2$ and is the driving force for the *C*49-to-*C*54 transformation, ΔG_S is the misfit strain energy caused by interfacial misfit between *C*49-$TiSi_2$ and *C*54-$TiSi_2$, and the coefficients *a*, *b*, and *c* have a particular set of values depending upon the specific geometries such as grain boundary (two-grain junction) and grain edge (three-grain junction). It can be seen from Eq. (7) that the more grain boundary eliminated, the lower the nucleation barrier. Based upon this energetic consideration, nucleation barrier at the grain edge is lower than that at the normal grain boundary. In other words, the grain-edge nucleation should be easier than the grain-boundary one. Our experimental results indicate that for thicker films (sample *C*) grain-boundary nucleation of the *C*54-$TiSi_2$ is the dominant mode, while grain-edge nucleation becomes dominant for thinner films (sample *A*). This seemingly anomalous transition implies that the nucleation of the *C*54-$TiSi_2$ becomes increasingly

difficult due to the thickness scaling: the higher-energy barrier grain-boundary nucleation mode was replaced by the lower energy barrier grain-edge nucleation one, where more grain-boundary energy eliminated can be used to compensate the extra energy barrier resulting from the reduction in the film thickness.

We suggest that there are at least two factors causing the increasing difficulty of the $C54$-$TiSi_2$ nucleation. One is the microstructure and morphology of the $C49$ phase which provides heterogeneous nucleation sites for the $C54$-$TiSi_2$; the other is the increasing surface-to-volume ratio associated with the thickness reduction. We postpone the discussion of the second factor to the next section. By comparing the morphology and microstructure features of samples A and C, the difference is obvious: the microstructure of the $C49$ phase in sample A (thinner films) can be viewed as a two-dimensional polygrain network with grains connected side by side, while that in sample C (thicker films) consists of at least one layer of $C49$ grains stacked over each other. This implies that the nucleation site density in sample A is much lower than that in sample C. As pointed out previously, the nucleation of the $C54$ phase mostly occurs inside the $C49$ disilicide matrix. Thus, we expect that these microstructure differences would affect the nucleation event in sample A (thinned films) because of the following reasons: (1) the greatly reduced heterogeneous sites for nucleating $C54$-$TiSi_2$, and (2) the restricted two-dimensional fluctuation for nucleation.

Houtum, Raaijmakers, and Menting[40] reported the influence of the $C49$-$TiSi_2$ grain size on the $C49$-to-$C54$ transformation. They observed that the transformation temperature decreases with reducing the grain size of the $C49$-$TiSi_2$. This result can be easily understood based upon our nucleation site density argument. For films of the same thickness, the decrease in grain size will greatly increase the density of heterogeneous nucleation sites. So the transformation can be facilitated due to the relative ease in nucleation. This aspect is extremely important for nucleation-controlled reaction process. Since nucleation is a fluctuation process and requires local mass transport even in the polymorphic transformation to reorder the structure, it is conceivable that such fluctuation is more limited to lateral direction in thinner films but has virtually no restriction in thicker films.

B. Effect of surface

Another factor which will influence the nucleation of the $C54$-$TiSi_2$ is the surface contribution. Decreasing film thickness largely increases the surface-to-volume ratio. In thinner films all volume elements are in close proximity to either a free surface or interphase boundary of some kind. Because of this fact, some of the interfacial energy $\sigma_{C49/C54}$ shown in Eq. (7) will be replaced by the surface energy σ_{C54} or interphase boundary energy $\sigma_{C54/\mathrm{Si}}$. But we propose that the most important effect of reducing the film thickness is the confinement of the shape of the nuclei. This confinement of dimensionality very effectively raises the nucleation barrier via largely increased surface-to-volume ratio, i.e., increasing b and reducing c in Eq. (7). To illustrate this concept, let us consider two kinds of geometrical shapes a $C54$-$TiSi_2$ nucleus will adopt: sphere and disk with the same volume. As shown in the Appendix, the disk-shaped nucleus has a larger surface-to-volume ratio than sphere-shape nucleus, so more energy will be needed to successfully create a disk-shaped $C54$-$TiSi_2$ nucleus. It is clearly demonstrated that simply by changing the surface-to-volume ratio, for example, from 3.63 to 5.72 (assuming that the radius of sphere is unity), the total surface (or interface) energy barrier will increase by nearly 60%. Following this reasoning, it is not difficult to think that nucleation in thinner films will require thermal activation at a higher temperature than in thicker films to overcome a higher energy barrier for creating a shape-confined $C54$-$TiSi_2$ nucleus. As shown in Figs. 1(a) and 1(b) (right), the grain-boundary grooving further reduces the effective thickness at these sites and thus restricts the shape of the nuclei. This is thought to be the cause for the difference observed between samples A and B. With further reducing the film thickness, a much higher temperature anneal will be required to convert the $C49$-$TiSi_2$ to the $C54$-$TiSi_2$. This is exactly the case recently reported by Jeon *et al.*[31] They found no occurrence of the $C54$ phase during annealing samples with Ti thickness below 200 Å at 900 °C. But in their case, in addition to the large surface contribution, other effects may also come into play such as degradation of the heterogeneous sites resulting from the islanding of the $C49$ grains.

Based upon these considerations, we can also explain the line width dependence of the $C49$-to-$C54$ transition observed by Lasky *et al.*[2] Due to the shrinkage of line width, nucleation site becomes very restricted and the site density is also greatly reduced. Furthermore, the shape confinement of the nucleus largely raises the energy barrier for the $C54$-$TiSi_2$ nucleation. All these factors resulted in the difficulty of the transformation.

C. Effect of stress

Although no stress information is available from these samples, we suggest that stress may also play a role in the understanding of the kinetic difference presented here. In thin film reactions, the effect of stress is usually ignored due to the large heat of formation of an intermetallic compound compared to relatively small contribution of stress. But in the case of the $C49$-to-$C54$ polymorphic transformation, the driving force is very small, stress contribution could be important for both nucleation and growth of the $C54$-$TiSi_2$. Stress in thin films typically comes from two parts: intrinsic stress and extrinsic stress. Intrinsic stress may originate from film deposition, interfacial reaction, and phase transformation. Interface misfit stress (or strain energy)[41,42] can also increase the nucleation barrier by reducing the denominator in Eq. (7). Extrinsic stress is related to thermal history of the samples and results from the difference in thermal expansion of the film and substrate. The combination of both effects usually generates relatively large biaxial stress in the film.

To find out the magnitude of these two stress com-

ponents, we estimated the elastic strain energy of the $C49$-$TiSi_2$ film at the elastic limit, i.e., the elastic strain at 0.2%, using the following equation:

$$E_{\mathrm{elastic}}=\int \sigma\, d\varepsilon=\tfrac{1}{2}Y\varepsilon^2\approx 2.6\times 10^{-5}\ \mathrm{eV/atom}\ , \quad (8)$$

where σ is the elastic stress and Y is the Young's modulus of $C49$-$TiSi_2$ ($=1.42\times 10^{12}$ dyn/cm^2).[43] This value is too small and can be neglected. Because the samples annealed in a conventional furnace is subjected to an initial transient heating before reaching isothermal temperature, the rapid transient heating to high temperature will introduce significant amounts of thermal stress in the film due to the slow stress relaxation process, which depends on the atomic diffusion. The effect of thermal stress on the kinetics of the transformation can be understood by evaluating the chemical potential change caused by different thermal-expansion coefficients of the film and substrate. Using the approach given by Rodbell *et al.*,[44] we obtained the chemical-potential change, $\sigma\Omega=0.026$ eV/atom,[45] where σ is the thermal stress of the $C49$-$TiSi_2$ film and Ω is the atomic volume of $C49$-$TiSi_2$. This chemical-potential change is very comparable to the expected driving force for the transformation. If there is not enough time to relax the stress, it will either hinder or enhance the transformation depending on the nature of the stress. Also, it can be expected that films of different thickness will have different stress values.

Very recently, Jongste *et al.*[46] have studied the formation of $C49$-$TiSi_2$ from Ti-Si multilayers with different periodicity using *in situ* stress measurements. They observed that after forming the $C49$ phase all films are under tensile stress. Their results also showed that films with small periodicity have higher tensile stress than those with large periodicity. This interesting observation made us suggest that the same trend of the stress state holds for our samples. Based upon the above estimation, we think that the higher tensile stress in thinner films is partially responsible for the observed higher activation energy for the transformation. Balluffi and Blakely[47] indicate that stress has a direct effect on atomic diffusion across interface via a change of activation volume. This will, in turn, affect the migration rate of the interface separating $C49$-$TiSi_2$ from $C54$-$TiSi_2$.[48] Obviously, stress measurements are needed to be carried out on these samples to substantiate this viewpoint.

V. CONCLUSION

We have demonstrated the large influence of the film thickness on the kinetics of the $C49$-$TiSi_2$-to-$C54$-$TiSi_2$ polymorphic transformation and the nucleation behavior of the $C54$ phase using *in situ* resistance measurements and TEM analysis. The results show a strong correlation between transformation temperature and film thickness, and between transformation temperature and transformation velocity. Kinetics analyses reveal that the activation energy of the transformation is a function of Ti film thickness, being equal to 3.73, 4.44, and 5.08 (± 0.07) eV for samples with 1000, 550, and 250 Å Ti, respectively. It has been shown that the increase in activation energy with reducing the film thickness is accompanied by an anomalous transition of the nucleation sites for the $C54$-$TiSi_2$ from a higher barrier grain boundary to a lower barrier grain edge. Based upon thermodynamic considerations, we have proposed that the $C49$-to-$C54$ transformation is limited by the nucleation of the $C54$ polymorph. The thickness dependence of the activation energy has been discussed by emphasizing the influence of film thickness on the nucleation of the $C54$-$TiSi_2$ in terms of energetics of nucleation at different sites, nucleation site density, and effects of surfaces and stresses. Using our simple geometrical model, we conclude that associated with the reduction in film thickness, the large increase in surface-to-volume ratio and restrictions in nucleation site are two major factors causing the increasing difficulty of nucleating the $C54$-$TiSi_2$. The observed site transition is a clear manifestation of this argument. It has also been suggested that stress may play a role in the observed kinetic difference.

ACKNOWLEDGMENTS

We very gratefully acknowledge the financial support from the Joint Services Electronics Program (JSEP) under Contract No. N00014-90-J-1270. Acknowledgment is also made to the donors of the Petroleum Research Fund, administered by the American Chemical Society. We wish to thank C. M. Wayman and E. Ma for many stimulating discussions. Thanks are also due to the Microelectronics Division of the NCR Corporation for providing us with the valuable samples employed in this study. Some of the materials characterizations were carried out at the Center for Microanalysis of Materials of the Materials Research Laboratory at the University of Illinois, which is supported by the U.S. Department of Energy (Division of Materials Science, Office of Basic Energy Sciences) under Grant No. DEFG02-91ER45439, and the U.S. National Science Foundation under Grant No. DMR-89-20538.

APPENDIX

Here we consider homogeneous nucleation of the $C54$-$TiSi_2$ in the $C49$-$TiSi_2$ matrix. The same derivation can be easily extended to the case of heterogeneous nucleation. It is assumed that the critical nucleus of the $C54$ phase takes the shape of a sphere in thicker films, which is also used as a reference for later comparison, and takes the shape of a disk in thinner films due to the restriction in vertical dimension. These are schematically shown in Fig. 10. Assume that both nuclei have the same

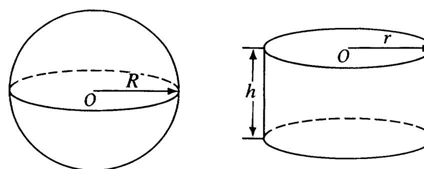

FIG. 10. Schematic diagram of the formation of (a) a spherical $C54$-$TiSi_2$ nucleus and (b) a disk-shaped $C54$-$TiSi_2$ nucleus within the $C49$-$TiSi_2$ thin films.

volume, i.e.,

$$\pi r^2 h = \tfrac{4}{3}\pi R^3$$

or

$$r^2 h = \tfrac{4}{3}R^3 . \tag{A1}$$

The surface-to-volume ratio obtained for the sphere-shaped nucleus is given by

$$\frac{A}{V} = \frac{4\pi R^2}{4/3\pi R^3} = \frac{3}{R} \tag{A2}$$

and for the disk-shaped nucleus is given by

$$\frac{A}{V} = \frac{2\pi r(r+h)}{\pi r^2 h} = 2\left[\frac{1}{h}+\frac{1}{r}\right] , \tag{A3}$$

where A is the whole surface area of the nucleus, V is the volume of the nucleus, r is the radius of the disk, h is the height of the disk, and R is the radius of the sphere.

There are two variables to fix the dimension of the disk. Because h and r are switchable in Eq. (A3), we consider only the change of h with respect to r. To demonstrate the effect of thickness on the surface-to-volume ratio and the associated nucleation energy barrier, we discuss the following three cases: (1) $h = r$, (2) $h = r/2$, and (3) $h = r/4$. Using these conditions and the relation in Eq. (A1), we obtain the surface-to-volume ratio of the disk-shaped nucleus:

$$\left[\frac{A}{V}\right]_{h=r} = \sqrt[3]{16/9}\,\frac{3}{R} \approx \frac{3.63}{R} , \tag{A4}$$

$$\left[\frac{A}{V}\right]_{h=r/2} = \sqrt[3]{3}\,\frac{3}{R} \approx \frac{4.33}{R} , \tag{A5}$$

$$\left[\frac{A}{V}\right]_{h=r/4} = \sqrt[3]{125/18}\,\frac{3}{R} \approx \frac{5.72}{R} . \tag{A6}$$

Their corresponding energy barrier can be expressed as

$$\Delta G^* = -\tfrac{4}{3}\pi R^3(\Delta G_V - \Delta G_S) + c4\pi R^2 \sigma_{C49/C54} , \tag{A7}$$

where ΔG^*, ΔG_V, ΔG_S, and $\sigma_{C49/C54}$ have the same meaning as those in Eq. (7). The coefficient c will have different values depending upon the shape and dimension of the nucleus, for example,

$$c_{\text{sphere}} = 1 ,$$

$$c_{h=r} = \sqrt[3]{16/9} \approx 1.21 ,$$

$$c_{h=r/2} = \sqrt[3]{3} \approx 1.44 ,$$

$$c_{h=r/4} = \sqrt[3]{125/18} \approx 1.91 .$$

[1]R. H. Dennard, F. H. Gaensslen, H. N. Yu, V. L. Rideout, E. Bassous, and A. R. Leblanc, IEEE J. Solid State Circuits **SC-9**, 256 (1974).

[2]J. B. Lasky, J. S. Nakos, O. J. Cain, and P. J. Geiss, IEEE Trans. Electron Devices **ED-34**, 575 (1987).

[3]S. Pramanick, Y. N. Erokhin, B. K. Patnaik, and G. A. Rozgonyi, Appl. Phys. Lett. **63**, 1933 (1993).

[4]C. M. Osburn, J. Electron. Mater. **19**, 67 (1990).

[5]C. A. Paszkiet, M. A. Korhonen, and C. Y. Li, in *Thin Films: Stresses and Mechanical Properties II,* edited by M. Doerner, W. C. Oliver, G. M. Pharr, and F. R. Brotzen, MRS Symposia Proceeedings No. 188 (Materials Research Society, Pittsburgh, 1990), p. 153.

[6]Q. Z. Hong, F. M. d'Heurle, J. M. E. Harper, and S. Q. Hong, Appl. Phys. Lett. **62**, 2637 (1993).

[7]C. Dehm, J. Gyulai, and H. Ryssel, Appl. Phys. Lett. **60**, 1214 (1992).

[8]R. Beyers, D. Coulman, and P. Merchant, J. Appl. Phys. **61**, 5110 (1987).

[9]R. Beyers and R. Sinclair, J. Appl. Phys. **57**, 5240 (1985).

[10]R. D. Thompson, H. Takai, P. A. Psaras, and K. N. Tu, J. Appl. Phys. **61**, 540 (1987).

[11]Z. Ma, L. H. Allen, and S. Lee, in *Interface Dynamics and Growth,* edited by K. S. Liang, M. P. Anderson, R. F. Bruinsma, and G. Scoles, MRS Symposia Proceedings No. 237 (Materials Research Society, Pittsburgh, 1992), p. 661.

[12]L. A. Clevenger, J. M. E. Harper, C. Cabral, Jr., C. Nobili, G. Ottaviani, and R. Mann, J. Appl. Phys. **72**, 4978 (1992).

[13]T. C. Chou, C. Y. Wong, and K. N. Tu, J. Appl. Phys. **62**, 2275 (1987).

[14]L. J. Chen and K. N. Tu, Mater. Sci. Rep. **6**, 53 (1991).

[15]K. H. Kim, J. J. Lee, D. J. Seo, C. K. Choi, S. R. Hong, J. D. Koh, S. C. Kim, J. Y. Lee, and M. A. Nicolet, J. Appl. Phys. **71**, 3812 (1992).

[16]W. Lur and L. J. Chen, J. Appl. Phys. **66**, 3604 (1989).

[17]Y. Matsubara, T. Horiuchi, and K. Okumura, Appl. Phys. Lett. **62**, 2634 (1993).

[18]Z. Ma, Y. Xu, L. H. Allen, and S. Lee, J. Appl. Phys. **74**, 2954 (1993).

[19]G. Ramanath, S. Koh, Z. Ma, L. H. Allen, and S. Lee, in *Rapid Thermal and Integrated Processing II,* edited by J. C. Gelpey, J. K. Elliott, J. J. Wortman, and A. Ajmera, MRS Symposia Proceedings No. 303 (Materials Research Society, Pittsburgh, 1993), p. 63.

[20]D. Turnbull and H. N. Treaftis, Acta Metall. **3**, 43 (1955).

[21]I. S. Servi and D. Turnbull, Acta Metall. **14**, 161 (1966).

[22]A. Cros, K. N. Tu, D. A. Smith, and B. Z. Weiss, Appl. Phys. Lett. **52**, 1311 (1988).

[23]G. Itoh and M. Kanno, in *Recrystallization '90,* edited by T. Chandra (The Mineral, Metals, Materials, Warrendale, PA, 1990), p. 579.

[24]A. R. Verma and P. Krishna, *Polymorphism and Polytypism in Crystals* (Wiley, New York, 1966).

[25]J. W. Christian, *The Theory of Transformations in Metals and Alloys, Part I,* 2nd ed. (Pergamon, Oxford, 1975).

[26]F. Nava, T. Tien, and K. N. Tu, J. Appl. Phys. **57**, 2018 (1985).

[27]F. Nava, B. Z. Weiss, K. N. Tu, D. A. Smith, and P. A. Psaras, J. Appl. Phys. **60**, 2445 (1986).

[28]J. W. Cahn, Acta Metall. **4**, 449 (1956).

[29]R. A. Vandermeer and R. A. Masumura, Acta Metall. **40**, 877 (1992).

[30]H. J. W. van Houtum and I. J. M. M. Raaijmakers, in *Thin Films-Interfaces and Phenomena,* edited by R. J. Memanich, P. S. Ho, and S. S. Lau, MRS Symposia Proceedings No. 54 (Materials Research Society, Pittsburgh, 1986), p. 37.
[31]H. Jeon, C. A. Sukow, J. W. Honeycutt, G. A. Rozgonyi, and R. J. Nemanich, J. Appl. Phys. **71**, 4269 (1992).
[32]X. H. Li, J. R. A. Carlsson, S. F. Gong, and H. T. G. Hentzell, J. Appl. Phys. **72**, 514 (1992).
[33]P. G. Cotter, J. A. Kohn, and R. A. Potter, J. Am. Ceram. Soc. **39**, 11 (1956).
[34]D. A. Robins and I. Jenkins, Acta Metall. **3**, 598 (1955).
[35]E. Ma, L. A. Clevenger, C. V. Thompson, and K. N. Tu, in *Thin Film Structures and Phase Stability,* edited by B. M. Clemens and W. L. Johnson, MRS Symposia Proceedings No. 187 (Materials Research Society, Pittsburgh, 1990), p. 83.
[36]P. M. Robinson and M. B. Bever, in *Intermetallic Compounds,* edited by J. H. Westbrook (Wiley, New York, 1967), p. 38.
[37]F. M. d'Heurle, J. Mater. Res. **3**, 167 (1988).
[38]F. M. d'Heurle, J. Vac. Sci. Technol. A **7**, 1467 (1989).
[39]P. J. Clemm and J. C. Fisher, Acta Metall. **3**, 70 (1955).
[40]H. J. W. van Houtum, I. J. M. M. Raaijmakers, and T. J. M. Menting, J. Appl. Phys. **61**, 3116 (1987).
[41]J. W. Cahn, Acta Metall. **28**, 1333 (1980).
[42]J. W. Cahn and F. Larche, Acta Metall. **30**, 51 (1982).
[43]J. F. Jongste, O. B. Loopstra, G. C. A. M. Janssen, and S. Radelaar, J. Appl. Phys. **73**, 2816 (1993).
[44]K. P. Rodbell, K. N. Tu, W. A. Lanford, and X. S. Guo, Phys. Rev. B **43**, 1422 (1991).
[45]I. A. Blech and C. Herring, Appl. Phys. Lett. **29**, 131 (1976).
[46]J. F. Jongste, P. F. A. Alkemade, G. C. A. M. Janssen, and S. Radelaar, J. Appl. Phys. **74**, 3869 (1993).
[47]R. W. Balluffi and J. M. Blakely, Thin Solid Films **25**, 363 (1975).
[48]D. Turnbull, J. Metals **3**, 661 (1951).

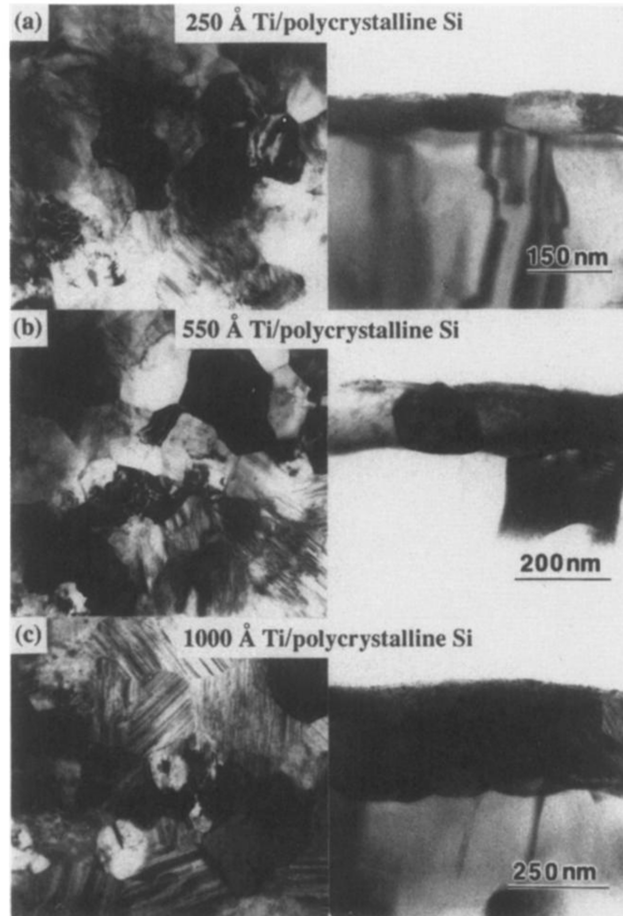

FIG. 1. Plan-view (left) and cross-sectional (right) TEM micrographs of the $C49$-$TiSi_2$ films formed by reacting poly-Si with Ti films of different thicknesses, showing the microstructure and morphology of the $C49$-$TiSi_2$ prior to transforming to the $C54$-$TiSi_2$. (a) 250 Å Ti, (b) 550 Å Ti, and (c) 1000 Å Ti.

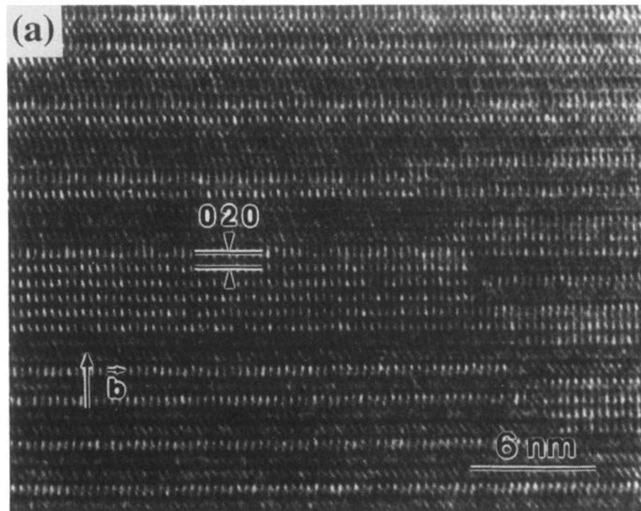

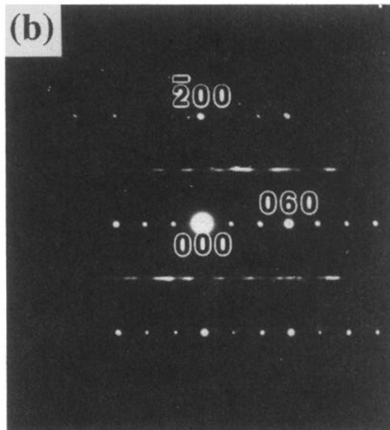

FIG. 2. (a) High-resolution TEM micrograph of the defective $C49$-$TiSi_2$ structure viewed along [100] axis. The stacking faults in **b** direction are revealed. The planes are often displaced by a vector $1/2(\mathbf{a}+\mathbf{c})$. (b) a typical [100] selected area electron-diffraction pattern.

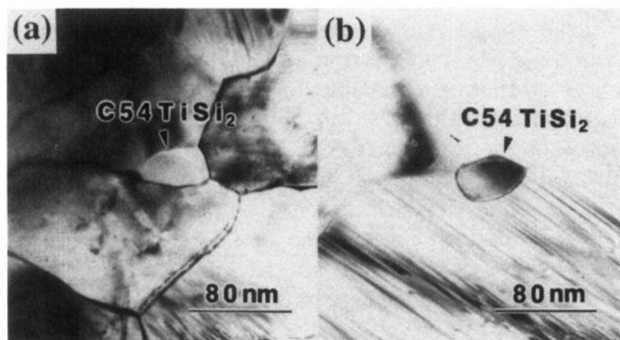

FIG. 9. Typical micrographs showing the location of the $C54$-$TiSi_2$ nuclei inside the $C49$-$TiSi_2$ thin films formed from samples with (a) 250 Å Ti (sample A) and (b) 1000 Å Ti (sample C). The $C54$ nuclei were identified using electron microdiffraction as well as dark-field imaging, and are indicated by arrows.